Computational study of flow around a simplified car body

Emmanuel Guilmineau

Computational study of flow around a simplified car body

Emmanuel Guilmineau

Laboratoire de Mécanique des Fluides, CNRS UMR 6598, Ecole Centrale de Nantes, Nantes, France

The Ahmed body is a simplified car used in automotive industry to investigate the influence of the flow structure on the drag. Wake flow is two-dimensional for low incidences of the rear slant, then becomes three-dimensional when the angle of the hatchback approaches 301 and reverts to two-dimensional behavior for angles higher than 301 where above this angle, a sudden drop in drag occurred. In this paper, we investigate numerically the flow around the Ahmed body for the base slant angles 251 and 351. Results are compared with experimental data. The two-dimensional behavior of the flow, for the slant angle 35, is well predicted, whereas the transition of the wake to a fully three-dimensional, for the slant angle 251, is not reproduced. Therefore, the flow around the Ahmed body with 251 slant angle can be considered an open challenge for turbulence modeling.

Keywords: Bluff body flow; Automotive aerodynamics; Turbulence simulation

1. Introduction

The study of three-dimensional flow around a ground vehicle has become a subject of significant importance in the automobile industry. One obvious way of improving the fuel economy of vehicles is to reduce aerodynamic drag by optimizing the body shape. Execution of good aerodynamic design under stylistic constraints requires an extensive understanding of the flow phenomena and, especially, how the aerodynamics are influenced by changes in body shape. The flow region which presents the major contribution

*Tel.: +33 2 40 37 16 81; fax: +33 2 40 37 25 23.
E-mail address: Emmanuel.Guilmineau@ec-nantes.fr

to a car's drag is the wake flow behind the vehicle. The location at which the flow separates determines the size of the separation zone, and consequently the drag force. Clearly, a more exact simulation of the wake flow and of the separation process is essential for the accuracy of drag predictions.

A real-life automobile is very complex shape to model or to study experimentally. However, the simplified vehicle shape employed by Ahmed et al. (1984) generates fully three-dimensional regions of separated flow which may enable a better understanding of such flows. Ahmed's body is 1044 mm long (L), 288 mm high and 389 mm width. The slant part is 222 mm long, whatever the angle. The bottom surface of the Ahmed body is located at 50 mm above the ground. This geometry is represented in Fig. 1. The flow around this body is strongly influenced by the angle of the rear slant surface, which indicates that the large portion of aerodynamic drag is generated by the development of three-dimensional vortex separation from the rear slant surface. The experimental data with this simplified car used in this paper are produced by Lienhart and Becker (2003). In these experiments, the flow velocity is $U_0 = 40\,\mathrm{ms}^{-1}$ and the kinematic viscosity of air $15 \times 10^{-6}\,\mathrm{m}^2\,\mathrm{s}^{-1}$. Then the Reynolds number, based on the body length, is 2.784×10^6. Two different rear body slant angles (25° and 35°) are considered, which happen to bracket the critical angle of 30° at which the drag is maximum. This drag crisis is due to a drastic change in the flow structure. The flow evolves, when increasing the angle from a quasi-two-dimensional wake to a complex three-dimensional very disipative structure. Past this critical angle, the wake becomes again quasi-two-dimensional. The incidence 35° corresponds to the low-drag configuration (quasi-two-dimensional wake) while the incidence 25° is the high-drag configuration (strongly three-dimensional wake). Simulations of flow around the Ahmed body were presented at two ERCOFTAC Workshops (Jakirlić et al., 2001; Manceau and Bonnet, 2002).

In this paper, we investigate numerically, with several turbulence models, the flow around the Ahmed body for both slant angles. Results are compared with experimental data of Lienhart and Becker (2003).

Fig. 1. Ahmed body view: (a) 25° rear slant; (b) 35° rear slant.

2. Flow solver

2.1. Navier–Stokes equations

The numerical simulation of stall control is performed by the ISIS flow solver, developed by EMN (Equipe Modélisation Numérique i.e. CFD Department of the Fluid Mechanics Laboratory). The prediction of massively separated flows, such as flows encountered in stall control, is a difficult task. Although large eddy simulation (LES) approaches may be more suitable for such flows, the present approach relies on solving unsteady Reynolds-averaged Navier Stokes equations (URANSE). Indeed, the computational cost of LES approaches is still prohibitive for high Reynolds numbers. Incompressible URANSE equations can be written as (using the generalized form of Gauss' theorem):

$$\frac{\partial}{\partial t}\int_V \rho \, \mathrm{d}V + \int_S \rho(\vec{U} - \vec{U}_d)\cdot\vec{n}\,\mathrm{d}S = 0, \tag{1a}$$

$$\frac{\partial}{\partial t}\int_V \rho U_i \, \mathrm{d}V + \int_S \rho U_i(\vec{U} - \vec{U}_d)\cdot\vec{n}\,\mathrm{d}S = \int_S (\tau_{ij}I_j - pI_i)\cdot\vec{n}\,\mathrm{d}S + \int_V \rho g_i \, \mathrm{d}V, \tag{1b}$$

where V is the domain of interest, or control volume, bounded by the closed surface S moving at the velocity $\vec{U}_d$ with a unit normal vector $\vec{n}$ directed outward. $\vec{U}$ and p represent, respectively, the velocity and pressure fields. τ_{ij} and g_i are the components of the viscous stress tensor and the gravity, whereas I_j is a vector whose components vanished, except for the component j which is equal to unity.

All the flow variables are stored at the geometric center of the arbitrary shaped cells. Volume and surface integrals are evaluated according to second-order accurate approximations. The various fluxes appearing in the discretized equations are built using centered and/or upwind schemes. For example, the convective fluxes are obtained by two kinds of upwind schemes. A first scheme available in the flow solver, (HD) for Hybrid differencing, is a combination of upwind (UD) and centered (CD) schemes. Contrary to a practical approach (Demirdžić and Muzaferija, 1995; Ferziger and Perić, 1996) where CD/UD blending is fixed with a global blending factor for all faces of the mesh, the HD scheme results from a local blending factor based on the signed Peclet number at the face. An other upwind scheme which is implemented in ISIS, is the gamma differencing scheme (GDS) (Jasak, 1996). Through a normalized variable diagram (NVD) analysis (Leonard, 1988), this scheme enforces local monotonicity and convection boundedness criterium (CBC) (Gaskell and Lau, 1988).

A pressure equation is obtained in the spirit of the Rhie and Chow procedure (Rhie and Chow, 1983). Momentum and pressure equations are solved in an segregated way like in the well-known SIMPLE coupling procedure (Patankar, 1980).

The temporal discretization is based on a three-step scheme ensuring a second-order accuracy. All spatial terms appearing in Eqs. (1a) and (1b) are discretized at the current time step, yielding an implicit scheme.

2.2. Turbulence modeling

Several turbulence closures are included in the flow solver, ranging from linear eddy-viscosity based models to full second-order closures (Duvigneau et al., 2003). With several models, we can choose a near-wall low-Reynolds version or wall function.

This first model selected is a quadratic explicit algebraic stress model proposed by Rumsey and Gatski (2001) that takes into account the production-to-dissipation rate ratio. It will be referred as EASM. This model relies on a three-term tensor bases which is not the exact explicit solution of the original algebraic stress model. EASM model for three-dimensional flow have been developed by Gatski and Speziale (1993). But the formulation is so complicated that it may be more expansive than the Reynolds stress transport model. In the present study, we prefer to solve implicitly the algebraic stress model proposed by Rodi (1976) (noted ASM). All of them base on the same pressure–strain correlation model, namely the quasi-linear SSG model (Gatski and Jongen, 2000). Both models are compared with their parent Reynolds stress transport model referred as RSM SSG model. Another

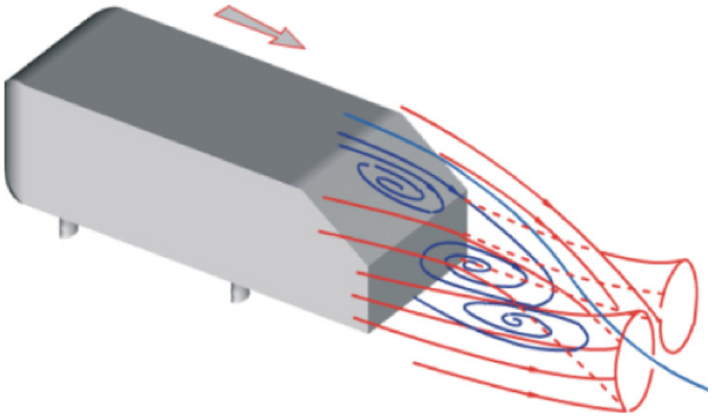

Fig. 2. Development of the flow for the 35° slant angle (courtesy of S. Becker and H. Lienhart).

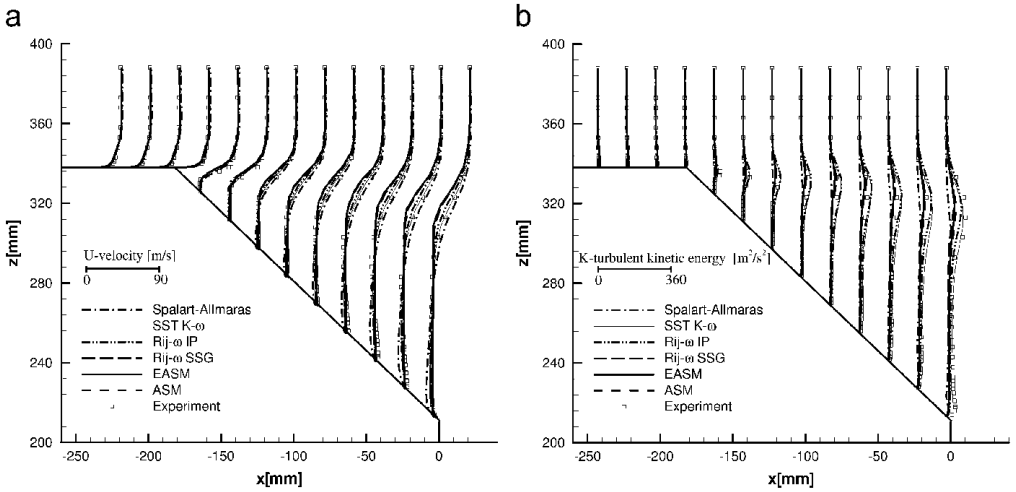

Fig. 3. 35°: velocity and turbulent kinetic energy profiles in the symmetric plane: (a) velocity; (b) turbulent kinetic energy.

pressure–strain correlation model has been proposed for the RSM: the isotropization-of-production model (IP). The RSM uses the turbulent frequency ω equation. Consequently, the RSM is referred $Rij-\omega$ IP or $Rij-\omega$ SSG according to the pressure–strain correlation model used. All these turbulence models are compared with a classical two-equation model the $k-\omega$ SST model proposed by Menter (1993) and the one-equation model the Spalart–Allmaras (1992).

All these turbulence models adopt a low-Reynolds number formulation. All turbulence models are implemented in the same house code, ISIS, using the same numerical method.

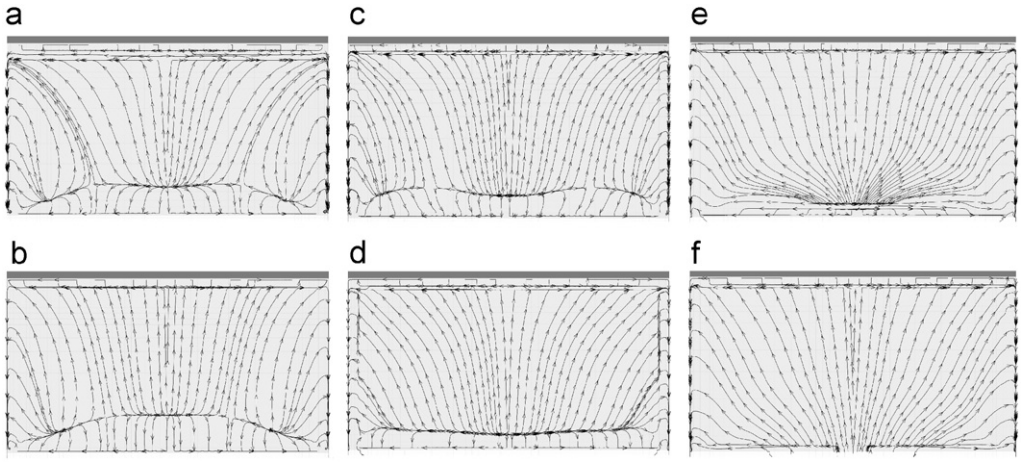

Fig. 4. 35°: friction lines on the rear slant (without stilts): (a) Spalart–Allmaras; (b) $K-\omega$ SST; (c) $R_{ij}-\omega$ IP; (d) $R_{ij}-\omega$ SSG; (e) EASM; and (f) ASM.

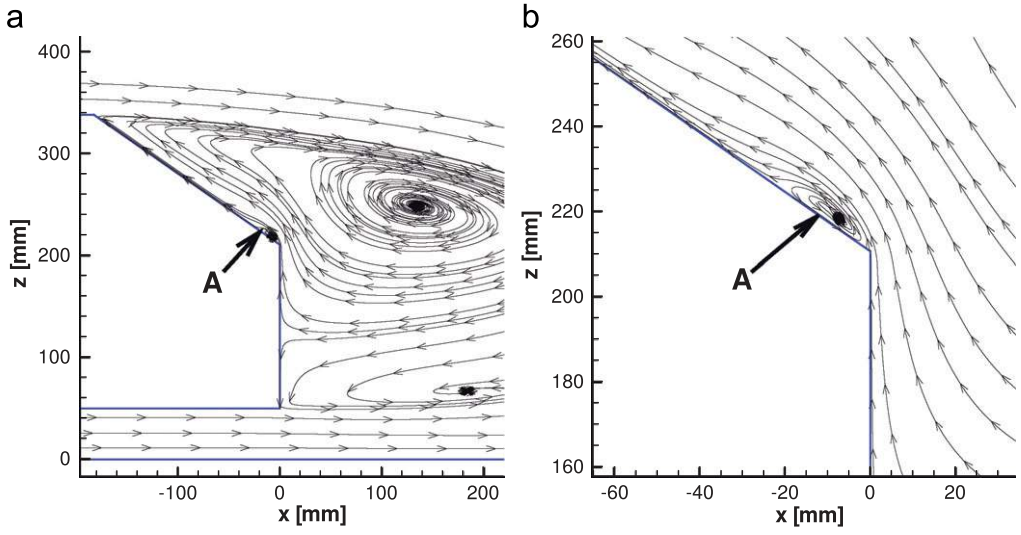

Fig. 5. 35°: streamlines in the symmetric plane: (a) general view; (b) zoom.

The incompressible URANSE are solved on an unstructured grid using a finite volume approach. The numerical implementation is detailed by Duvigneau et al. (2003).

3. Grid description

The computational domain is defined by the half body. It starts at two body length in front and three body lengths behind the Ahmed body. The width of the domain is 0.935 m and the height is 1.4 m. The body is located at 50 mm above the plane. The center of the coordinate system is placed at the end of Ahmed body ($x = 0$ end of the model, $y = 0$ symmetric plane, $z = 0$ ground plane). The half-body assumption is used because the model is symmetric and the researched solution is a steady flow. In experiments, the flow is three-dimensional and unsymmetric in an unsteady sense with the mean being symmetric.

The grid without stilts is composed to 1.8×10^6 points and employed 16 blocks while with stilts it is composed to 3.6×10^6 points and employed in 32 blocks. The Ahmed body is described by 15,300 points. Due to the low-Reynolds turbulence model, the distance between the first fluid points and the walls is fixed to 0.005 mm. Then, the distance y^+ is near to 0.25. However, the number of grid points in the boundary layer is approximately 30.

4. Numerical results

For both slant angles, we search a steady flows. So, the first term in Eqs. (1a) and (1b) is null. Consequently, the non-linear iteration number is the alone parameter to determine the convergence of the solution. In this study, the non-linear iteration number is 10,000.

4.1. Rear slant angle: 35°

Experimentally, the two counter-rotating vortices are weak, the separation occurs along the entire slant and there is no reattachment on the slant. An illustration of the experimental flow is illustrated by the sketch given in Fig. 2.

The center-line profiles of the mean-velocity and turbulent kinetic energy over the rear slant are plotted in Figs. 3(a) and (b), respectively. All turbulence models predict the fully separated of this flow-field. There are no significant differences between results except at

Table 1
Drag coefficient versus turbulence models for both slant angles

	35°		25°	
	Without stilts	With stilts	Without stilts	With stilts
Spalart–Allmaras	0.3404	×	0.3291	×
SST $K-\omega$	0.2895	0.3133	0.3074	×
$R_{ij}-\omega$ IP	0.2835	0.3115	0.3016	×
$R_{ij}-\omega$ SSG	0.2504	0.2849	0.2698	×
EASM	0.2356	0.2668	0.2138	×
ASM	0.2364	0.2710	0.2505	×
Experiment (Ahmed et al., 1984)	×	0.260	×	0.285

the end of the rear slant with the Spalart–Allmaras model. For the turbulent kinetic energy, all turbulence models used the SSG pressure–strain correlation model give similar result and underestimate the turbulent kinetic energy.

Fig. 4 present the frictions lines on the slant part of the whole Ahmed body for all turbulence models used. We can see that the patterns are very similar. Some differences

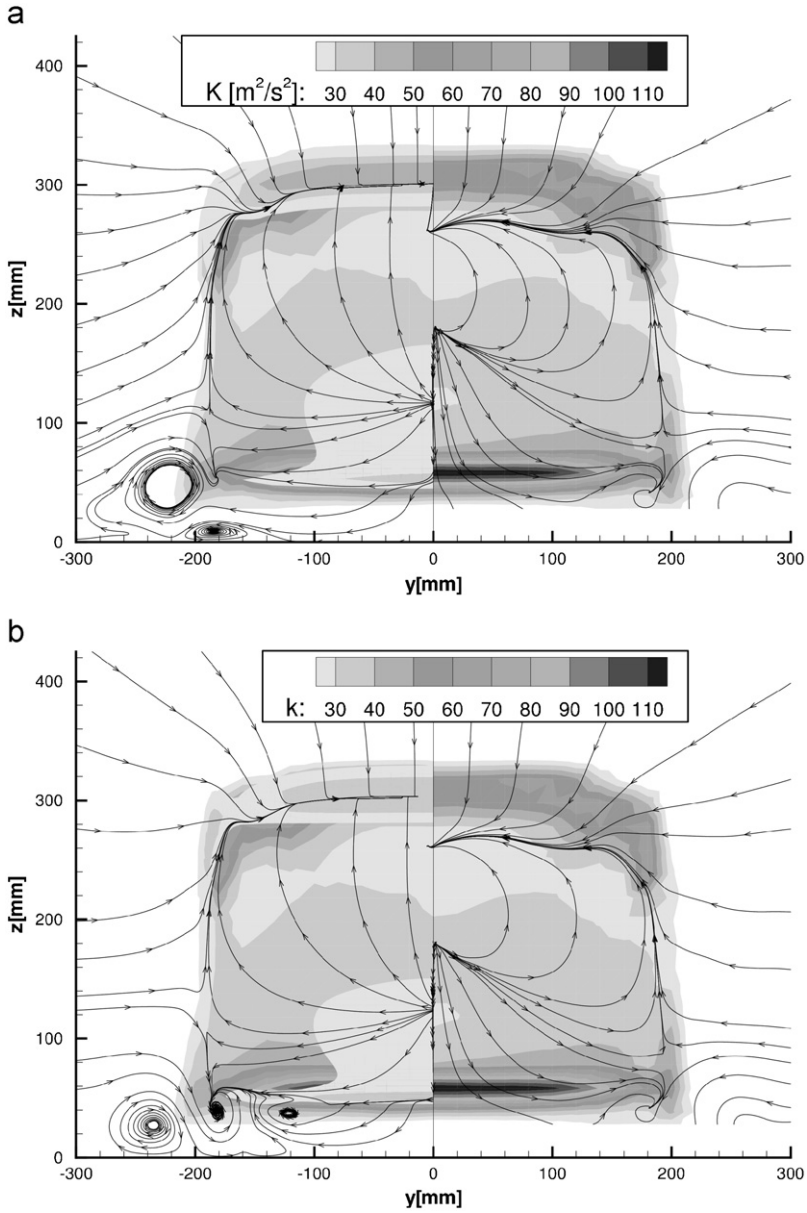

Fig. 6. 35°: turbulent kinetic energy and streamlines at $x = 80$ mm: (a) without stilts (left), experiment (right); (b) with stilts (left) experiment (right).

exist for the position of the reattachments and the intensity of the bottom corner vortex, noted (A), as shown in Fig. 5 which present the streamlines in the symmetric plane.

Table 1 compares the drag coefficients predicted by the present computations to the experimental measurements of Ahmed et al. (1984). We can notice that simulations with the EASM model and the stilts give a good prediction of the experimental drag. The predicted value is less than 3% of the experimental value. The algebraic turbulence models give better results. The Spalart–Allmaras model overestimate dramatically the drag, even without the stilts. In this case, the predicted value is higher than 32% of the experimental data. As the simulation obtained with the EASM turbulence model gives a better prediction of the drag, we choice this turbulence model to characterize the influence of the presence of the stilts in the wake.

Fig. 6 chart the wake at a position $x = 80\,\text{mm}$ by the turbulent kinetic energy and the streamlines of the secondary flow. Experimental measurements are compared to those predicted by the EASM model, without the stilts on which the model was supported in the wind tunnel (Fig. 6(a)) and with (Fig. 6(b)). With stilts, the turbulent kinetic energy is higher than without around the bottom of the model, near the ground. Contours of turbulent kinetic energy show a poor agreement in the wake of the body. The topology of the wake is well predicted. As the recirculation is more extended in the computation than the experiments, the both counter-rotating vortices are less intense in the numerical simulation than in experiments.

4.2. Rear slant angle: 25°

Experimentally, the two strong counter-rotating vortices emanating from the slant are present and the flow separates in the middle region of the top edge and reattaches on the slant. An illustration of the experimental flow is illustrated by the sketch given in Fig. 7. Consequently, the turbulence model must predict separation and reattachment on the slant.

Fig. 8(a) shows the center-line profiles of the mean-velocity and Fig. 8(b) the turbulent kinetic energy. All turbulence models do a very poor prediction of the flow. Although all

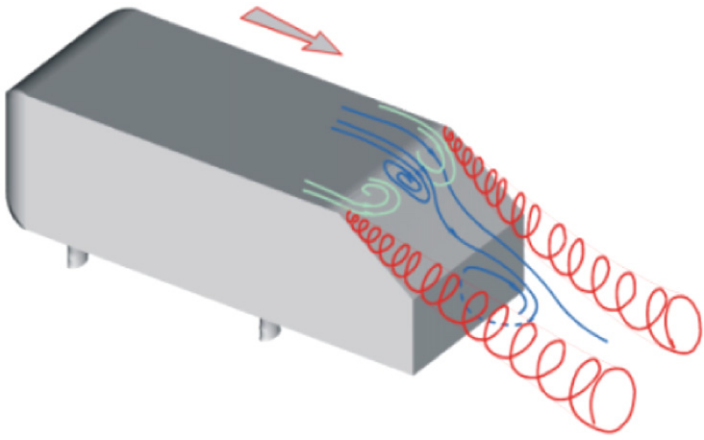

Fig. 7. Development of the flow for the 25° slant angle (courtesy of S. Becker and H. Lienhart).

models, except the Spalart–Allmaras model for which the flow remains attached, predict separation just past the top of the slant, as in experiment, neither predicts the same reattachment seen in the experiment.

The friction lines over the slant surface are shown in Fig. 9 for all turbulence models. All models using the SSG closures and $K-\omega$ SST predict a similar result. The difference is the trace of the longitudinal vortices. With the Spalart–Allmaras model, these vortices are strong and cover the end of the rear slant. While with the $R_{ij}-\omega$ IP model, the flow structure is very different. There exists an arch above the slant. These differences are due to the intensity of the longitudinal vortex. We thus note that there are three types of topology: that obtained with the Spalart–Allmaras model, that obtained with the $R_{ij}-\omega$ IP model and the others which are very similar. Fig. 10 present a comparison, at $x = 80$ mm, of the

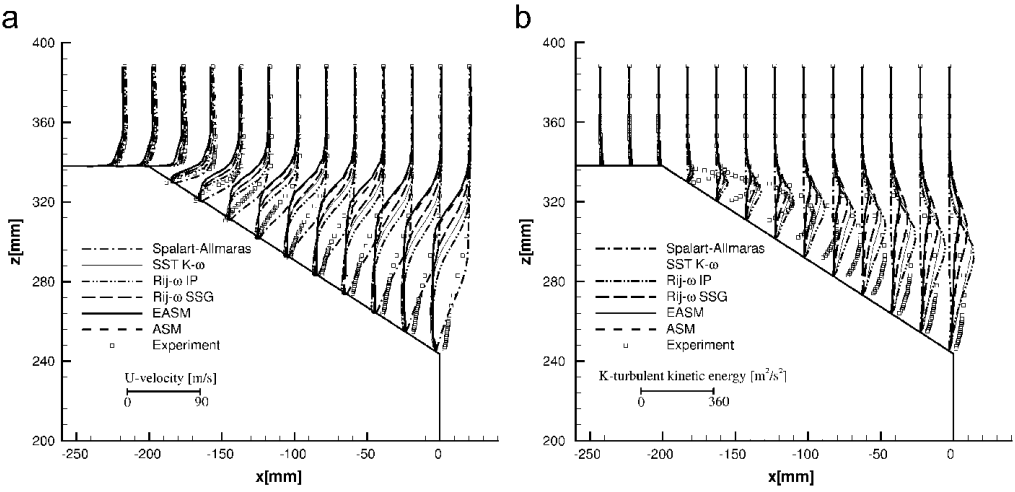

Fig. 8. 25°: velocity and turbulent kinetic energy profiles in the symmetric plane: (a) velocity; (b) turbulent kinetic energy.

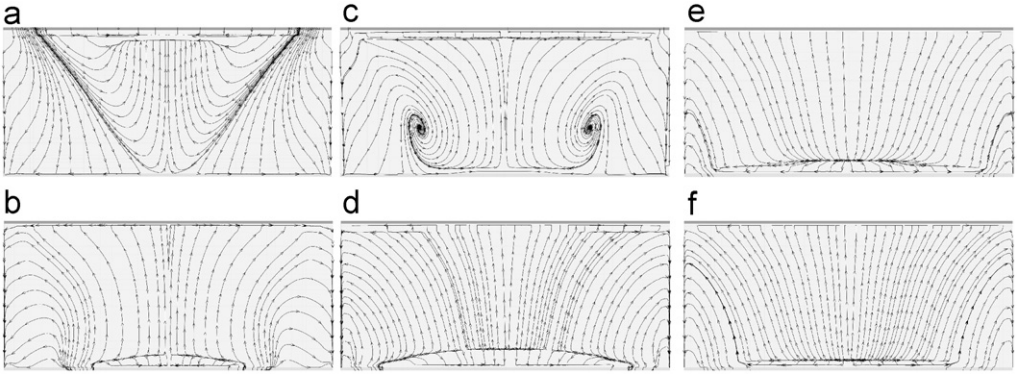

Fig. 9. 25°: friction lines on the rear slant (without stilts): (a) spalart–Allmaras; (b) $K-\omega$ SST; (c) $R_{ij}-\omega$ IP; (d) $R_{ij}-\omega$ SSG; (e) EASM; and (f) ASM.

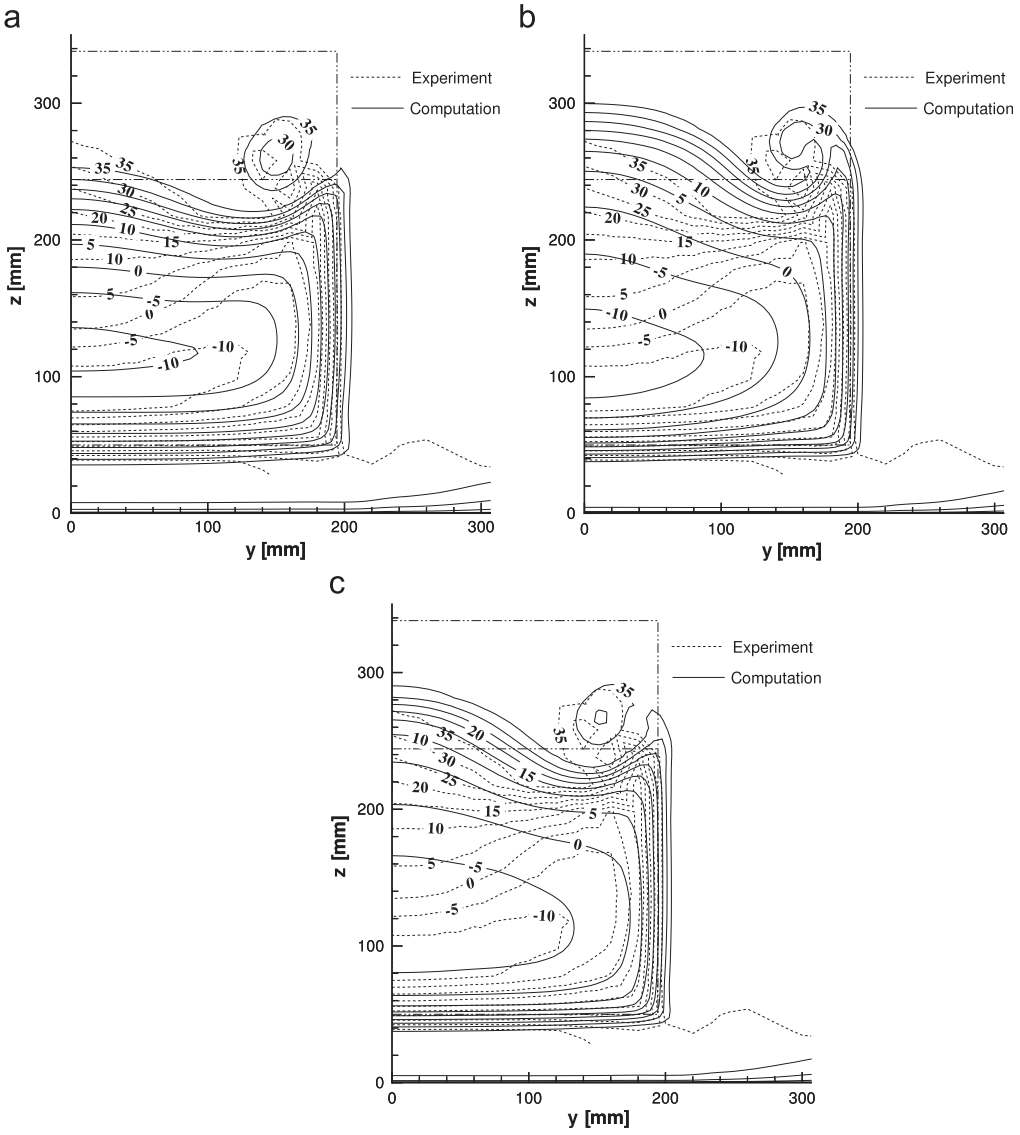

Fig. 10. 25°: iso-velocity at $x = 80$ mm: (a) Spalart–Allmaras; (b) $K-\omega$ SST; and (c) $R_{ij}-\omega$ IP.

iso-velocity between experiments and numerical results, for the Spalart–Allmaras model (Fig. 10(a)), for the $K-\omega$ SST model (Fig. 10(b)) and for the $R_{ij}-\omega$ IP model (Fig. 10(c)). Of these figures, one notices that the longitudinal vortex obtained with the Spalart–Allmaras model is too intense compared to that measured in experiments. For the $K-\omega$ SST model, simulation predicts a vortex which is not intense enough compared to the experiment. These differences in intensity of the longitudinal vortex explain the differences of the friction lines obtained on the rear window.

5. Conclusions

Simulations, with several turbulence models, have been carried out for the generic Ahmed body with 25° and 35° slant angles. For the larger slant angle, computations with or without the stilts on which the body was supported in the wind tunnel give similar results. However, the drag is increased due to the presence of the stilts. All turbulence models predict the topology of the flow correctly. On the other hand, the EASM model gives a better estimate of the drag. By taking of account the stilts, this model gives a value to less than 3% of the experimental value. At the 25° slant angle, all simulations predict massive separation, whereas the experiment shows reattachment about half-way down the center of the face. This case continues to pose strong challenges to the turbulence modeling.

Acknowledgments

The authors gratefully acknowledge the scientific committee of CINES (project dmn2049) and IDRIS (project 129) for the attribution of CPU time.

References

Ahmed, S.R., Ramm, G., Faltin, G., 1984. Some salient features of the time-averaged ground vehicle wake, SAE Technical Paper 840300.

Demirdžić, I., Muzaferija, S., 1995. Numerical method for coupled fluid flow, heat transfer and stress analysis using unstructured moving meshes with cells of arbitrary topology. Comput. Methods Appl. Mech. Eng. 125, 235–255.

Duvigneau, R., Visonneau, M., Deng, G.B., 2003. On the role played by turbulence closures in hull ship optimization at model and full scale. J. Mar. Sci. Technol. 8, 11–25.

Ferziger, J.H., Perić, M., 1996. Computational Methods for Fluid Dynamics. Springer, Berlin.

Gaskell, P.H., Lau, A.K.C., 1988. Curvature-compensated convective transport: SMART, a new boundedness preserving transport algorithm. Int. J. Numer. Methods Fluids 8, 617–641.

Gatski, T.B., Jongen, T., 2000. Nonlinear eddy viscosity and algebraic stress models for solving complex turbulent flows. Prog. Aerosp. Sci. 36, 655–682.

Gatski, T.B., Speziale, C.G., 1993. On explicit algebraic stress models for complex turbulent flows. J. Fluid Mech. 254, 59–78.

Jakirlić, S., Jester-Zürker, R., Tropea, C. (Eds.), 2001. In: 9th Joint ERCOFTAC/IAHR/QNET-CFD Workshop on Refined Turbulence Modelling.

Jasak, H., 1996. Error analysis and estimation for the finite volume method with applications to fluid flows. Ph.D. Thesis, University of London.

Leonard, B.P., 1988. Simple high-accuracy resolution program for convective modelling of discontinuities. Int. J. Numer. Methods Fluids 8, 1291–1318.

Lienhart, H., Becker, S., 2003. Flow and turbulence structure in the wake of a simplified car model. SAE Technical Paper 2003-01-0656.

Manceau, R., Bonnet J.P., (Eds.), 2002. In: 10th Joint ERCOFTAC/IAHR/QNET-CFD Workshop on Refined Turbulence Modelling.

Menter, F.R., 1993. Zonal two-equation $k-\omega$ turbulence models for aerodynamic flows. In: AIAA 24th Fluid Dynamics Conference, Orlando, FL. AIAA Paper 93-2906.

Patankar, S.V., 1980. Numerical Heat Transfer and Fluid Flow. Hemisphere Publishing Corporation, New York.

Rhie, C.M., Chow, W.L., 1983. A numerical study of the turbulent flow past an isolated aerofoil with trailing edge separation. AIAA J. 17, 1525–1532.

Rodi, W., 1976. A new algebraic relation for calculating the Reynolds stresses. ZAMM 56, 219–222.

Rumsey, C.L., Gatski, T.B., 2001. Recent turbulence model advances applied to multielement airfoil computations. J. Aircr. 38, 904–910.

Spalart, P., Allmaras, S., 1992. A one-equation turbulence model for aerodynamic flows. In: AIAA 30th Aerospace Sciences Meeting, Reno, NV. AIAA Paper 92-0439.